FTIR Spectroscopic Investigation of the Mechanism and Kinetics of the Heterogeneous Reactions of NO_2 and HNO_3 with Soot

U. Kirchner,* V. Scheer, and R. Vogt*

Ford Forschungszentrum Aachen GmbH, Süsterfeldstrasse 200, D-52072 Aachen, Germany

Received: February 10, 2000; In Final Form: July 19, 2000

Soot samples from a spark generator, a flame, and a diesel passenger car were either collected on a Teflon filter and transferred to an IR-transparent window or deposited directly from a flame onto the window and investigated by Fourier transform infrared (FTIR) spectroscopy. The soot-covered windows were mounted in a 10 cm vacuum cell connected to a standard flow system with He as carrier gas. Reactive gases, such as NO_2 and HNO_3, were added to the carrier gas flow at a concentration of (0.016 to 2.5) $\times$ 10^{14} molecule cm^{-3}. FTIR spectra of soot samples before and after exposure to HNO_3, NO_2, and O_3 are presented. Formation of IR absorption bands was analyzed as a function of exposure time. IR bands attributable to soot surface oxidation products and nitrogen containing species, e.g. −C═O, R−NO_2, R−ONO_2, and R−ONO were observed. The observed time dependence of the absorption bands of the spark generator soot can be fitted by two parallel reactions, a slow and a fast process. Both processes have a reaction order of $n \approx 0.2$ (± 0.3) for the NO_2 + soot reaction and $n \approx 0.5$ (± 0.6) for the HNO_3 + soot reaction. The number of active sites, $N_{max} = 2.2 \times 10^{14}$ molecules cm^{-2} soot surface, has been estimated from saturation experiments. Surface reaction probabilities depend on reactant concentration and reaction time and were in the range of $\gamma \approx 10^{-6}$ to 10^{-8} for the slow, and $\gamma \approx 10^{-3}$ to 10^{-6} for the fast processes. The reaction probability on diesel engine soot was nearly 1 order of magnitude slower. It is concluded that the reaction of NO_2 with soot cannot account for the HONO levels observed in urban air.

Introduction

Carbonaceous aerosol particles and NO_x compounds are produced simultaneously by combustion of fossil fuels and biomass. In model studies carbonaceous aerosols are considered to serve as heterogeneous reaction sites in the atmosphere.[1−3] Their reactivity, hygroscopic behavior, and potential catalytic activity are expected to depend on the nature of the functional chemical groups covering the surface of the particles. A representation of a hexane soot segment showing graphitic carbon layers and functional groups can be found in the literature.[4,5] Diesel soot consists not only of graphitic carbon but also a significant portion of organic carbon. A mass ratio of organic carbon to elemental carbon of up to 0.5 has been reported.[6] For a diesel engine running at idle, this ratio can even be higher.[7] Freshly emitted diesel soot particles are hydrophobic and water insoluble. Upon oxidation, soot becomes more hygroscopic, which may be one fundamental step for the removal of soot aerosol from the atmosphere by wet deposition.[8,9] Because of its high absorption cross section, carbonaceous aerosol is expected to influence light absorption and radiative transfer in the atmosphere.[10] In model calculations it was concluded that the global impact is likely to be a cooling effect.[10] To better understand the aerosol properties and atmospheric effects it is important to investigate the fundamental chemical processes occurring on the soot surface.

In the reaction of NO_2 with soot, the formation of different gas-phase products has been observed. HONO can be a major reaction product depending on the NO_2 concentration and relative humidity.[11−15] In many investigations NO was observed as a gas-phase product.[16−18] At high NO_2 concentrations (160 mbar) the products NO and N_2O were found in the reaction of *n*-hexane soot.[19] Much less is known about the change of the physical and chemical surface properties of the reacting soot. The loss of NO_2 from the gas phase has been investigated in Knudsen cell studies at low concentrations of NO_2.[16,17] Adsorption products were directly observed by infrared spectroscopy at high NO_2/N_2O_4 concentrations in the range of 6.7 mbar and 320 mbar.[20] Using isotopically labeled NO_2 functional groups, such as carboxylic C═O, C−ONO and C−NO_2 have been identified.

HNO_3 has been reported to react with soot,[18,21] whereas NO is unreactive.[22,23] However, little is known on the reaction mechanism and processes occurring on the soot surface. The complexity of soot surface reactions including the mechanism and kinetics of elementary reactions has recently been described by Kamm et al.[24] for the reaction of ozone with soot aerosol.

Here we present a study using well-characterized samples of spark generator soot which has also been used in other studies. A comparison of prior studies illustrates that different types of soot react differently with NO_2 and yield different reaction products.[15] Due to the various sources of ambient carbonaceous aerosol there are most probably many types of soot in the

* To whom correspondence should be addressed.

10.1021/jp0005322 CCC: $19.00
Published on Web 09/13/2000

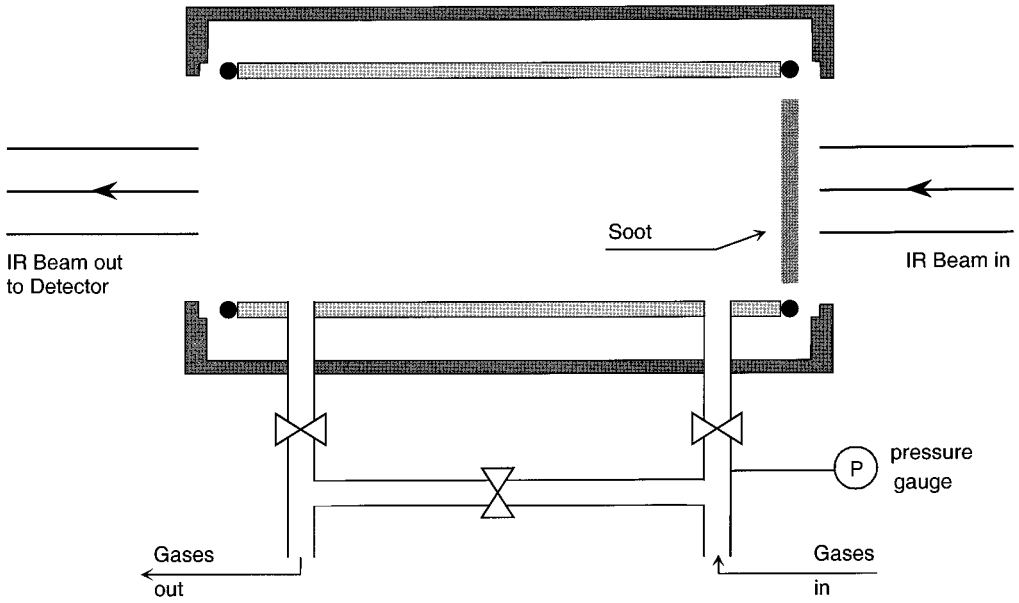

Figure 1. Schematic of the FTIR cell with ZnSe windows.

atmosphere, and it will be difficult to choose an ideal representative for ambient carbonaceous aerosol.

Experimental Section

All IR spectra were measured at 4 cm^{-1} resolution using a Bruker Equinox 55 FTIR spectrometer equipped with an MCT detector. A 10 cm transmission cell with 25 mm diameter optical windows was placed into the sample compartment and was connected to a standard flow system (Figure 1). The cell was equipped with a capacitance manometer (MKS, model 626 A) and Teflon valves to direct the gas flows either through a bypass to adjust the flows and concentrations, or through the cell. One window of the cell was covered with soot, transmission spectra were recorded relative to the evacuated cell as reference. Spectra were recorded by averaging 100 scans, which gave a time resolution of about 30 s in the typical wavenumber range from 4000 to 600 cm^{-1}. Helium (> 99.999%, Messer Griesheim GmbH, Germany) with a flow rate in the range from 4 to 20 $cm^3\ min^{-1}$ (at standard pressure) was used as carrier gas, which typically resulted in a cell pressure of 1 to 3 mbar. Reactive gases were added to the carrier gas flow from a calibrated 500 mL Pyrex glass bulb, in which the pressure was kept constant for 24 h by connecting to a 6 L reservoir bulb. By measuring the pressure drop with a pressure gauge (MKS, model 690 A) the concentration in the cell was determined. Concentrations of NO_2 in the range of (0.016 to 2.5) $\times$ 10^{14} molecule cm^{-3} (70 ppbv to 17 ppmv referred to ambient pressure) were employed. All used gases were dry.

NO_2 was prepared from NO (Messer Griesheim, purity > 99.5%) and O_2 (Messer Griesheim, purity > 99.998%) in a cleaned and passivated 1 L glass bulb. Both compounds were further purified by slowly passing the gases through a cold trap at −80 °C. The reaction product was further purified by distillation. No absorption bands of compounds other than NO_2 were visible in the IR. Considering the thermodynamic equilibrium, 2 $NO_2 \rightleftharpoons N_2O_4$, the N_2O_4 content is <0.01% under our experimental conditions.[25]

Gaseous HNO_3 was prepared by mixing 1 mL concentrated H_2SO_4 and 1 mL fuming HNO_3 (>90%), which was subsequently purified by several freeze−pump−thaw cycles. The outgassing HNO_3 was immediately mixed with He in a passivated storage bulb. Potential impurities, such as NO_2, N_2O, N_2O_3, and N_2O_5, were <1% as examined by FTIR.

Ozone was continuously produced in a flow of 100 $cm^3\ min^{-1}$ synthetic air by illumination with a mercury lamp at ambient pressure. After further dilution the concentration was measured using a UV ozone analyzer (model 400, API Inc.). At a constant flow the ozone concentration was 40 ppmv (1×10^{15} molecule cm^{-3}).

Most soot samples, which are subsequently referred to as "GfG soot" were prepared using a commercial spark generator (model GfG 1000, Palas GmbH, Germany). In this instrument a pulsed discharge is applied to two graphite electrodes. The aerosol generator was operated at a discharge rate of 300 Hz and an argon flow rate of 5.2 l min^{-1} (Messer Griesheim, Ar > 99.999%, N_2 < 5 ppmv, O_2 < 2 ppmv and H_2O < 3 ppmv). For some experiments the Ar was further purified using an adsorber tube filled with chromium(II)oxide (Oxisorb, Messer Griesheim; specified to reduce impurities of O_2 < 0.1 ppmv and H_2O < 0.5 ppmv). The production of NO_x in the plasma of the spark discharge from impurities in the Ar or in the graphite electrodes was measured using a NO_x analyzer (model 200A, API Inc.). It was found to be always below 10 ppbv (with ≈50% NO). The soot aerosol was passed into a bulb from which samples were collected on PTFE filters (pore size 0.2 μm, Sartorius). After a sampling time of 8 min, about 150 μg of soot was collected on the filter.

In some experiments the aerosol was further diluted with humidified synthetic air (40 to 80% relative humidity) and stored in a 500 L Teflon bag prior to sampling on the filter. Probing the aerosol from the Teflon bag with a scanning mobility particle sizer (SMPS model 3934, DMA 3071A, and CPC 3010, TSI Inc.) showed a well reproducible log-normal size distribution with a maximum electrical mobility diameter of 80 nm. After collection on filters and transfer to optical windows, all soot samples were treated with dry gases.

For comparison, samples were collected from various other sources using the same filters and setup as described above: commercial carbon black (FW2, Degussa) was resuspended using a brush aerosol generator (model RBG-1000, Palas GmbH); exhaust from a diesel engine passenger car; and soot from a flame burning hexane or diesel fuel. Different regions

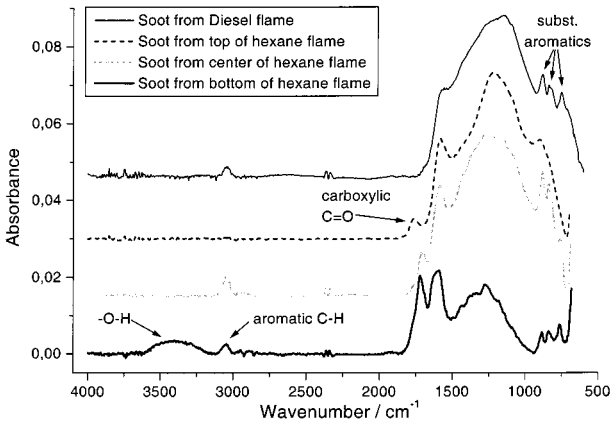

Figure 2. IR spectra of soot samples deposited from different flames and IR band assignments. Spectra are baseline corrected, intensity normalized, and shifted for clarity. Absorptions between 2380 and 2300 cm^{-1} are due to gaseous CO_2 in the spectrometer because of purge fluctuations and should be neglected.

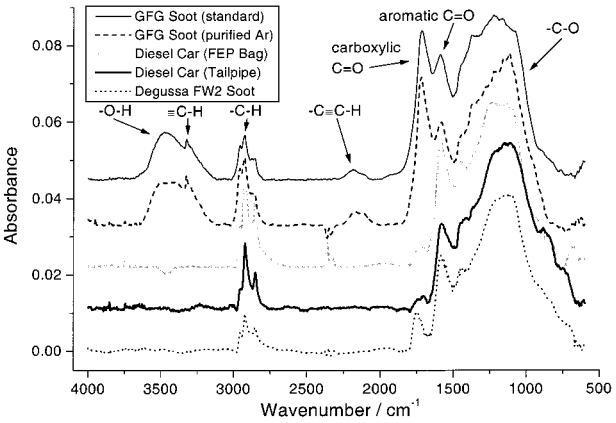

Figure 3. IR spectra of filter samples of soot from different sources and assignments of IR bands. Spectra are baseline corrected, normalized, and shifted for clarity. Absorptions of gaseous CO_2 between 2380 and 2300 cm^{-1} are due to small changes in the spectrometer purge and should be neglected.

of the flame were probed by placing a ZnSe or BaF_2 window directly into the flame at different positions.

Results

Absorption Spectra of Unreacted Soot Samples. FTIR spectra of flame and filter deposited soot samples obtained from various sources are displayed in Figure 2 and Figure 3. The most intensive absorption features can be attributed to oxygenated functionalities, such as −C−O, aromatic −C═O and carboxylic −C═O groups.[26,27] The underlying absorption of the carbon skeleton, i.e., −C−C− and −C═C− groups, results in a broad combination of peaks between 800 and 1600 cm^{-1}. This broad band might already contain signals of reaction products of the most reactive sites with trace gases, which were generated during aerosol production. However, significant spectroscopic differences are observed among the soot samples: a weak −O−H group can be found only in hexane soot sampled from the bottom of a flame, while all other hexane and diesel flame soot samples do not show this absorption feature. Aromatic −C−H bonds at 3050 cm^{-1} and −C═O groups, both carboxylic and aromatic at 1720 and 1600 cm^{-1}, respectively, appear in most spectra, but with varying intensities. Substituted aromatics at 880, 840, and 760 cm^{-1} [28] can be found in all flame-deposited

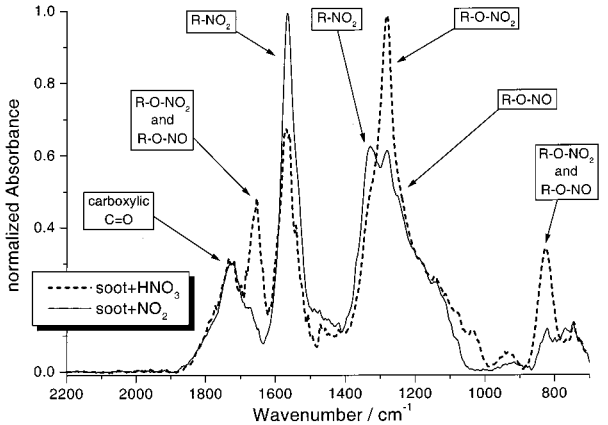

Figure 4. Product spectra of GfG soot + NO_2 and GfG soot + HNO_3 with proposed band assignments. Each plot is an average of six independent experiments with different NO_2 and HNO_3 concentrations at long reaction times (≈1000 min).

soot samples, but with very low intensity in hexane soot from the top of the flame. Olefinic ═C−H bands would also absorb at 3050 cm^{-1}; however, because the absorption band is always observed in conjunction with bands of substituted aromatics, the attribution to aromatic −C−H bands appear to be more likely. A possible explanation for the occurrence of aromatics in soot from the bottom region of the flame is that the aromatics may not form or may react further in the oxidizing top region of the flame. The composition of soot samples depends on sampling conditions.

The most obvious difference observed in soot aerosol samples collected on a filter (Figure 3) compared to flame deposited samples (Figure 2) are the missing substituted aromatics bands and the occurrence of aliphatic C−H vibrations at 2800 to 3000 cm^{-1} in the filter samples. This is probably an effect of the flame which is in contact with the soot and the cold surface during the deposition process. No difference is observed in diesel engine soot sampled directly from the tailpipe or sampled after dilution and collection in a Teflon bag. Only in Palas GfG soot samples were C≡C−H group features at 3320 cm^{-1} and at 2100−2200 cm^{-1}, and an intense O−H group around 3500 cm^{-1} observed. All bands and their intensities appear independently of a further purification of the argon from O_2 and H_2O using a special cartridge (Oxisorb, Messer Griesheim). Therefore, it is likely that the impurities originate from the graphite electrodes. Spectra of different amounts of GfG soot show that the absolute value of the absorbance depends, within experimental error, linearly on the soot mass.

We have chosen GfG soot as model substance because its physical properties, i.e., size distribution and chemical composition, are highly reproducible and because it has been used widely in other studies.[29,12] Nevertheless, it is not an ideal representative for diesel engine soot as seen in the significant differences of the IR spectra. Hexane flame soot, which has been used in several studies before, shows strong spectroscopic variations depending on the sampling conditions. Even soot from a diesel fuel flame is not a simple model substance because of the different chemical groups observed in IR spectra that might have an impact on the reaction rates.

Products of the Reaction of NO_2 and HNO_3 with Soot. GfG soot samples deposited on a ZnSe window were exposed to NO_2 (0.016 to 2.5 × 10^{14} molecule cm^{-3}) and nitric acid (0.054 to 2.2 × 10^{14} molecule cm^{-3}). Product spectra of the reactions are displayed in Figure 4. The unreacted soot was taken

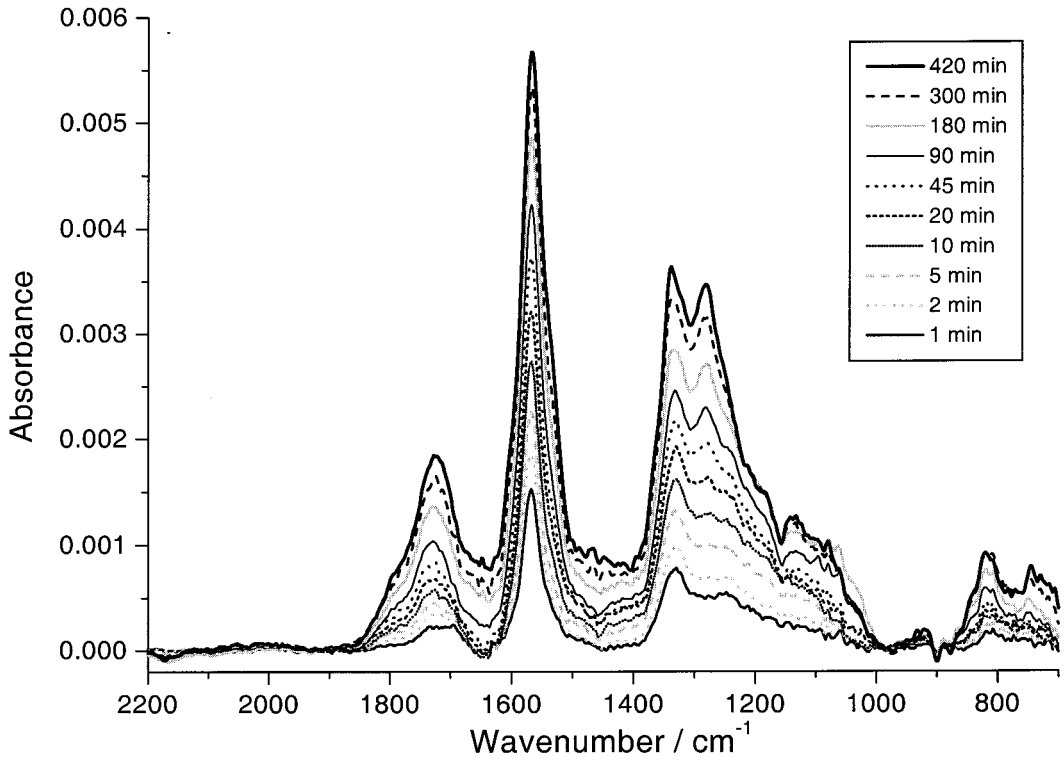

Figure 5. IR absorption bands observed during the reaction of GfG soot with NO_2. (Typical experimental conditions were: $[NO_2] = 7 \times 10^{13}$ molecule cm^{-3}, carrier gas flow = 20 cm^3 min^{-1} He, p(cell) = 2.2 mbar, mass(soot) = 145 μg on ZnSe window.)

as the reference spectrum; the change of absorbance shown in Figure 4 is caused by reaction of the soot with NO_2 and HNO_3. Spectra of products of the NO_2 and HNO_3 + soot reaction are compared in Figure 4. Absorption bands of an organic nitrate, R−O−NO_2 (1660, 1280, and 825 cm^{-1}) and a nitro compound R−NO_2 (1565 and 1320 cm^{-1}) were identified.[19,20] Similar absorption bands are observed in both reactions, with the exception that intensities of the nitrate bands, R−O−NO_2, were higher in the soot + HNO_3 reaction while the intensities of bands attributed to nitro compounds, R−NO_2, were higher in the soot + NO_2 reaction.

In Figure 5 the product absorption as a function of time is shown for a typical soot + NO_2 experiment. The product absorbance was observed to be linearly dependent on the soot mass, i.e., sample thickness and is independent of the NO_2 concentration. This supports that the entire internal surface is available for reaction and is probed by the IR beam. The absorption changes rapidly during the initial phase of the reaction. However, the surface becomes totally saturated at the end of an experiment, which typically takes about 1000 min. After 5 to 7 h of reaction time some absorption bands in the range of 3000 to 2700 cm^{-1} become visible, which we believe arise from an organic impurity in the vacuum system which slowly adsorbs on the soot surface. To check for further absorption bands arising from impurities, the experiment was repeated several times under the same flow conditions but without NO_2. It was shown that the wavenumber range from 1700 to 1480 cm^{-1} was entirely free of interference, and therefore the most intense band peak around 1570 cm^{-1} was chosen for quantitative analysis.

In addition to the bands shown in Figure 4, a decrease of the broad IR absorption at ∼3500 cm^{-1} was observed, indicating the consumption of OH groups on the soot surface. This indicates oxidation reactions and ester formation for which the following net reactions can be given.

$$2R{-}OH + 3NO_2 \rightarrow 2R{-}ONO_2 + NO + H_2O$$

$$3R{-}CH_2{-}OH + 2NO_2 \rightarrow 2R{-}CH_2{-}NO_2 + R{-}HC{=}O + 2H_2O$$

$$\text{for R = phenyl: } \Delta_r H = -288.5 \text{ kJ mol}^{-1}$$

$$R{-}CH_2{-}OH + NO_2 \rightarrow R{-}HC{=}O + NO + H_2O$$

$$\text{for R = phenyl: } \Delta_r H = -154 \text{ kJ mol}^{-1}$$

$$R{-}CH_2{-}OH + 2NO_2 \rightarrow R{-}HC{=}O + 2HONO$$

$$\text{for R = phenyl: } \Delta_r H = -151.7 \text{ kJ mol}^{-1}$$

$$R{-}H + 2NO_2 \rightarrow R{-}NO_2 + HONO$$

$$\text{for R = phenyl: } \Delta_r H = -182.5 \text{ kJ mol}^{-1}$$

$$R{-}OH + HNO_3 \rightleftharpoons R{-}ONO_2 + H_2O$$

If R is a phenyl group, the simplest surrogate for the aromatic system of soot, then for some reactions the reaction enthalpy, $\Delta_r H$, can be calculated.[30] Most likely, all of the above reactions are exothermic. To compare the soot surface oxidation products GfG soot and diesel soot were exposed to 40 ppmv ozone in synthetic air. The product spectra in Figure 6 show absorption bands which are due to O−H, C=O and C−O groups at ∼3500, 1720, and ∼1300 to ∼900 cm^{-1}, respectively, and consumption of C−H in the range 3000 to 2800 cm^{-1}.

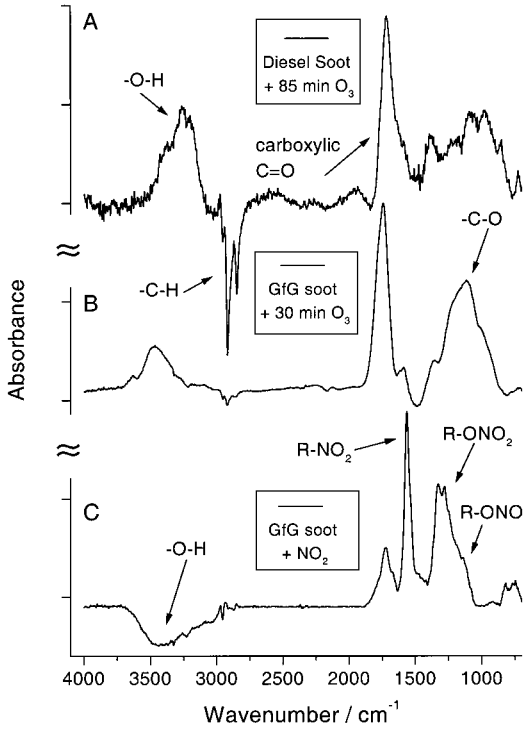

Figure 6. Product spectra for reactions of GfG and diesel soot with ozone (A and B) and GfG soot with NO_2 (C). The formation of similar oxygenated functional groups and consumption of hydrocarbons are visible upon oxidation by ozone. The difference spectrum of GfG soot before and after reaction with NO_2 (C) shows increasing bands of C═O, R−NO_2, R−ONO_2 and R−ONO (see also Figure 4) and a decreasing O−H band.

These bands are in good agreement with spectra described in the literature.[5,26,8] Surprisingly, the O−H, C═O, and C−O bands are already contained in the unreacted GfG soot (Figure 3). The most probable explanation may be impurities in the graphite of the electrodes. Another possibility is formation of O atoms in the spark discharge from O_2 traces in the Ar gas flow which may react with the soot. However, using further purified argon did not change the intensity of absorption bands which are due to oxygenated species so that this explanation is less likely. The strong absorption bands at 1660, 1565, ~1300, or at 830 cm^{-1} (Figures 4 and 5) are attributable to R−ONO_2/R−ONO, R−NO_2, R−ONO_2, and R−ONO_2/R−ONO groups, respectively. Interestingly, the band at 1720 cm^{-1} is observed in both the O_3 and the NO_2 reaction. The band originates from a non-nitrogen containing oxidation product and is attributed to carboxylic C═O.

To check for the reversibility of the NO_2 interaction, the reacted soot was pumped for up to 3 h to $< 10^{-2}$ mbar and then purged with He for 2 h. No change in absorption intensity occurred, showing that the observed products are strongly bonded rather than just physisorbed.

Kinetics of the NO_2 + Soot Reaction. In Figure 7 the integrated peak area of the R−NO_2 band between 1600 and 1510 cm^{-1} is shown for three different soot samples exposed to [NO_2] in the range from 1.1×10^{13} to 1.7×10^{13} molecule cm^{-3}. The peak intensities scale approximately linearly with the soot mass. Diesel soot, which was collected from the exhaust of a diesel passenger car and exposed to NO_2, showed very similar absorption bands as GfG soot. The mass of the diesel soot sample is comparable to the GfG soot sample displayed in the upper line in Figure 7. The integrated absorbance of the band at 1600−1510 cm^{-1} is roughly a factor of 7 lower, which

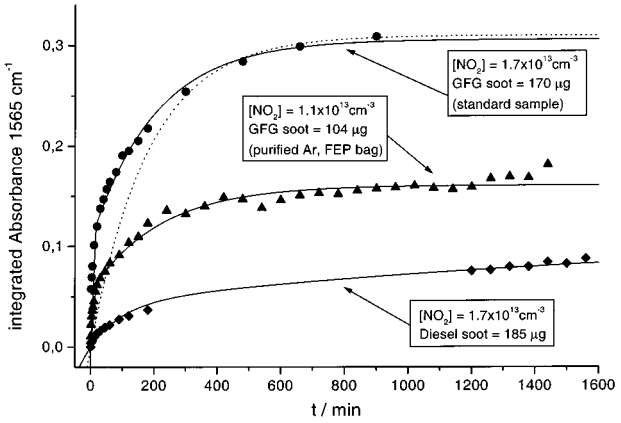

Figure 7. Integrated absorbances of the IR band at 1565 cm^{-1} for runs with different soot samples and soot masses and similar NO_2 concentrations. The solid lines are fits using two saturation reactions as described in the text; the dotted line is a fit using only one saturation reaction.

illustrates the lower reactivity and lower available specific surface area of diesel soot.

From Figure 7 it can be seen that the integrated peak absorbances in the reaction NO_2 + GfG soot saturate at long reaction times. A surface saturation reaction with one type of reactive site, S_r, can be described by the following equations:

$$S_r(t) + NO_2 \xrightarrow{k_r} \text{Prod.} \quad (1)$$

$$dProd./dt = k_r S_r(t)[NO_2]^n \quad (2)$$

$$S_r(t) \propto P_\infty - P \quad (3)$$

$$dP/dt = k_r^*(P_\infty - P)[NO_2]^n \quad (4)$$

where $S_r(t)$ is the number of reactive sites, Prod. is the number of product sites, n is the reaction order, k_r^* is the reaction rate constant, P is the integrated absorbance of product bands divided by the soot mass, and P_∞ is the integrated absorbance of product bands divided by the soot mass after surface saturation.

Integration of eq 4 leads to eq 5:

$$P(t) = P_\infty (1 - \exp(-k_r^*[NO_2]^n t)) \quad (5)$$

A fit of the experimental data shows significant deviations from eq 5, especially at short reaction times (see dotted line in Figure 7). However, the experimental data can be fitted much better (see solid lines in Figure 7) if we assume an additional, much faster saturation reaction of a second type of reactive sites, S_{ini}, which has the same reaction product absorption bands:

$$S_r(t) + NO_2 \xrightarrow{k_r} \text{Prod.} \quad (1)$$

$$S_{ini}(t) + NO_2 \xrightarrow{k_{ini}} \text{Prod.} \quad (6)$$

where k_{ini}^* is the reaction rate constant of initial reaction, k_r^* is the reaction rate constant of long-time reaction r, and where $k_r \ll k_{ini}$. Addition of the integrated forms of both reaction equations leads to eq 7:

$$P(t) = FP_\infty(1 - \exp(-k_{ini}^*[NO_2]^n t)) + (1 - F)P_\infty(1 - \exp(-k_r^*[NO_2]^n t)) \quad (7)$$

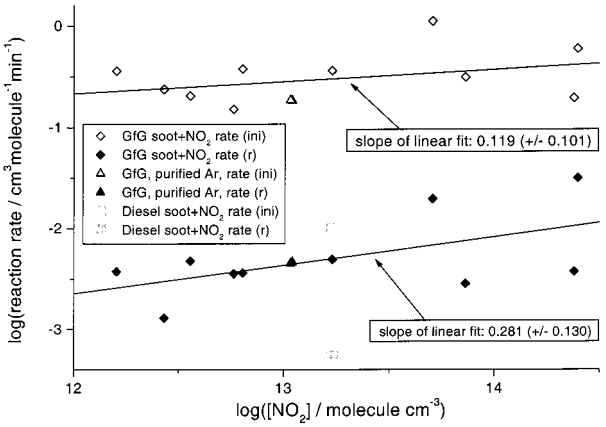

Figure 8. Reaction rates (ini) and (r) for the reactive soot sites S_{ini} and S_r in NO_2 + GfG soot as a function of NO_2 concentration. The fast reaction with rates (ini) are marked with hollow symbols, the slow reaction with rates (r) with filled symbols. In two experiments (triangles) GfG soot was used which was generated using purified Ar for the spark discharge. The reaction rates determined from the fit to the experimental data did not differ from those determined with soot generated using the usual Ar of a purity of 99.999%. The slope of the linear fit gives the reaction order.

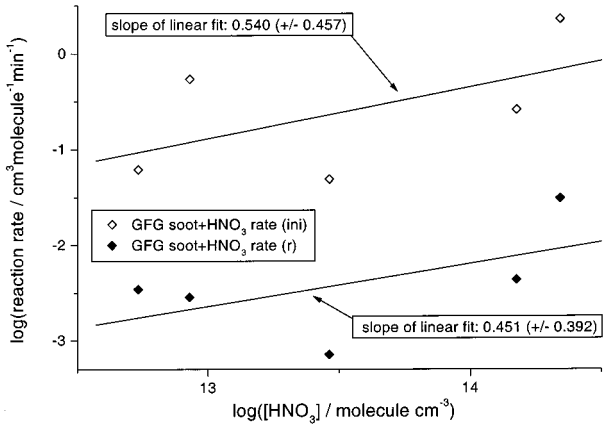

Figure 9. Reaction rates (ini) and (r) for the reactive soot sites S_{ini} and S_r in HNO_3 + GfG soot as a function of HNO_3 concentration. From the slopes of the linear fits the reaction order of $n \approx 0.5$ for both the slow and the fast reaction is determined.

where $F = P_{ini,\infty}/P_\infty$ is the contribution of reaction ini to the total absorbance and $(1 - F) = P_{r,\infty}/P_\infty$ is the contribution of reaction r to the total absorbance.

The reaction order in NO_2, n, may be determined from the slope of a bilogarithmic plot of the reaction rates (ini) and (r) and the NO_2 concentration (Figure 8).[31] The reaction orders of the two processes are $n_{ini} = 0.12$ (± 0.3) for the fast process (ini) and $n_r = 0.28$ (± 0.3) for the slow process (r). The given error is the sum of statistical and estimated experimental uncertainties based on the reproducibility of the result of an experiment. These results are in good agreement with a recently published work in which a reaction order of $n = 0$ was found for the reaction NO_2 + GfG soot for reaction times of up to 150 s in the concentration range around 12 ppbv.[12]

The data points obtained in a reaction using GfG soot which was prepared with purified Ar for the spark discharge fit well into this data series. In an experiment using diesel soot directly sampled from the tailpipe of a passenger car, the fitted reaction rates are nearly 1 order of magnitude smaller than those determined for GfG soot. This might have two reasons: First, the exhaust gas contains about 1.5 ppmv (3.7×10^{13} molecule cm^{-3}) NO_2, and the soot particles were in contact with the exhaust gas during their residence in the tailpipe at high temperature and on the filter during sampling. Therefore, they may already have reacted with NO_2 and only the second part of the overall reaction is observed. Second, the GfG soot has a specific surface area of 200 $m^2\ g^{-1}$,[29] whereas the diesel soot surface area is about 50 $m^2\ g^{-1}$.[32] A smaller surface area means fewer reactive sites on a soot sample with the same mass and same number of active sites per surface unit, resulting in fewer adsorbed NO_2 molecules and therefore in smaller absorption bands.

Kinetics of the HNO_3 + Soot Reaction. The same set of GfG soot experiments was conducted with HNO_3 as reactive trace gas. The integrated absorbances in the reaction HNO_3 + soot follow a saturation very similar to that seen for NO_2 + soot (Figures 5 and 6). The most intensive peak is located at about 1280 cm^{-1} (Figure 4), from which a background signal originating from an organic impurity had to be subtracted at reaction times longer than 5 to 7 h. Therefore, the second intensive band at about 1565 cm^{-1} was used for integration and quantitative analysis, which is the same as in the soot + NO_2 reaction. As for the NO_2 reaction, the data from the HNO_3 reaction can be fitted best if two parallel reactions with rate (ini) for a fast and rate (r) for a slow process are assumed. The scatter of the data points in Figure 9 is larger because of experimental difficulties using the sticky compound HNO_3, which results in more unstable concentrations during the reaction. Linear regression of the data points yields reaction orders of $n_{ini} = 0.54$ (± 0.6) and $n_r = 0.45$ (± 0.6) for rate (ini) and rate (r), respectively, which is not considerably higher than in the corresponding NO_2 reaction. Therefore, both reactions probably follow similar mechanisms.

Surface Reaction Probabilities. A reaction order close to zero indicates a complex reaction mechanism that consists of at least two steps: a very fast concentration independent adsorption of gas phase species onto the soot surface followed by a rate limiting reaction on the surface which consists of a slower and a faster process with reactive sites (r) and (ini), respectively. Although the reaction probability, γ, is defined for first-order reactions only, at small concentration intervals it is possible to apply eq 8:

$$\gamma = \frac{\text{reactive collisions}}{\text{total collisions}} = \left(\frac{dP}{dt} \cdot \frac{N_{max}}{FP_\infty}\right) \Big/ \left(^1/_4 \bar{c} A_{soot} [NO_2]\right) \quad (8)$$

where A_{soot} is the accessible surface area of the soot sample ($mass_{soot} \times 200\ m^2 g^{-1}$), $\bar{c}$ is the molecular velocity (NO_2: 370 ms^{-1}; HNO_3: 316 ms^{-1}), N_{max} is the maximum number of active sites on soot which can be covered by NO_2 molecules (4.4×10^{17} sites/mg soot).

The accessible surface area of the GfG soot, 200 $m^2 g^{-1}$, was taken from Kamm et al. (1997)[29] and Kamm et al. (1999).[24] For fresh GfG soot the surface area is roughly a factor of 2 smaller than the BET surface area.[24] The maximum number of NO_2 molecules that can adsorb per mg of soot, N_{max}, was determined in a separate experiment in which the amount of NO_2 lost from the gas phase was measured after surface saturation had occurred.[33] In this study it was observed that 1.9×10^{15} molecule cm^{-3} NO_2 react with a soot mass of 187 μg in a closed cell with a volume of 41.5 cm^{-3} using an initial concentration of $[NO_2] = 2.6 \times 10^{15}$ molecule cm^{-3}. Considering the soot surface area $A = 200\ m^2\ g^{-1}$, the number of reactive sites $S = 4.4 \times 10^{17}$ molecule/mg soot, or $N_{max} = 2.2 \times 10^{14}$ molecules per cm^2 soot surface, can be calculated.

TABLE 1: Reaction Probabilities of NO_2 + GfG Soot at Different NO_2 Concentrations for the Fast Reaction (ini) and the Slow Reaction (r)

$[NO_2]$	γ (ini)	γ (r)
2.4×10^{14}	1.5×10^{-6}	1.6×10^{-8}
7.3×10^{13}	1.2×10^{-5}	6.4×10^{-8}
1.7×10^{13}	8.0×10^{-5}	5.7×10^{-7}
1.1×10^{13}	9.2×10^{-5}	1.2×10^{-6}
1.1×10^{13}	1.2×10^{-4}	1.6×10^{-6}
6.4×10^{12}	2.1×10^{-4}	6.5×10^{-7}
5.8×10^{12}	1.0×10^{-4}	1.3×10^{-6}
2.7×10^{12}	5.0×10^{-4}	1.1×10^{-6}
1.6×10^{12}	1.7×10^{-3}	6.1×10^{-6}

TABLE 2: Reaction Probabilities of HNO_3 + GfG Soot at Different HNO_3 Concentrations for the Fast Reaction (ini) and the Slow Reaction (r)

$[HNO_3]$	γ (ini)	γ (r)
2.2×10^{14}	2.8×10^{-5}	7.8×10^{-7}
1.5×10^{14}	5.2×10^{-6}	1.1×10^{-7}
2.9×10^{13}	5.7×10^{-6}	9.8×10^{-8}
8.5×10^{12}	7.7×10^{-4}	1.0×10^{-6}
5.4×10^{12}	2.3×10^{-4}	1.9×10^{-6}

The surface reaction probabilities for the formation of the spectroscopically observed reaction products are estimated according to eq 8 and vary between $\gamma \approx 2 \times 10^{-3}$ and $\gamma \approx 2 \times 10^{-6}$ for the fast process if $[NO_2]$ is varied from 1.6×10^{12} molecule cm^{-3} to 2.4×10^{14} molecule cm^{-3}. The reaction probability of the slow process varies from $\gamma \approx 6 \times 10^{-6}$ to $\gamma \approx 2 \times 10^{-8}$ in the same concentration range. If we assume the same number of reactive sites, N_{max}, for HNO_3, the reaction probability varies from $\gamma \approx 8 \times 10^{-4}$ to $\gamma \approx 5 \times 10^{-6}$ for the fast process and from $\gamma \approx 2 \times 10^{-6}$ to $\gamma \approx 1 \times 10^{-7}$ for the slow process at $[HNO_3] = 5.4 \times 10^{12}$ molecule cm^{-3} to 2.2×10^{14} molecule cm^{-3}. The data are summarized in Table 1 and Table 2.

The values of the surface reaction probability, γ(r), observed in this work are in agreement with Kamm et al. (1997),[29] who determined the reactive uptake coefficient $\gamma < 10^{-7}$ for the uptake of NO_2 on GfG soot in an aerosol chamber at reaction times of several days. Kleffmann et al. (1999)[14] measured the formation of HONO and found γ in the range of 10^{-9} to 10^{-7} in an experiment in which 45 mg soot were exposed to $[NO_2] = 15$ ppmv (3×10^{14} molecule cm^{-3}). Their experimental NO_2/soot ratio of 8.7×10^{19} molecule g^{-1} may be compared to atmospheric conditions (10 μg m^{-3} soot, 10 ppbv NO_2), which corresponds to a NO_2/soot ratio of 2.5×10^{22} molecule g^{-1}. Kleffmann et al. (1999)[14] argue that although the absolute NO_2 concentration is 3 orders of magnitude higher than in the atmosphere, the experimental conditions are still relevant to atmospheric conditions.

In our study the corresponding ratio is $\approx 2.5 \times 10^{21}$ molecule g^{-1} (100 μg soot, $\approx$1 ppmv NO_2, 10 cm^3 min^{-1}, 1000 min), which is well below the atmospheric ratio although the absolute NO_2 concentration is about 100 times higher. It is interesting to note that our reaction probability for the formation of surface nitro groups corresponds well to the HONO formation rate of Kleffmann et al. (1999).[14] This is an indication that such surface nitro groups might play a key role during the formation of HONO on soot surfaces.

Ammann et al. (1998)[12] studied the HONO formation rate on GfG soot in an aerosol flow reactor for short reaction times of up to 150 s and with $[NO_2]$ in the low ppbv range. Their reported value of $\gamma \approx 10^{-4}$ is comparable with our γ (ini). In experiments using a Knudsen cell, values for the uptake coefficient of $\gamma = 0.11$ for NO_2 + soot and $\gamma = 0.038$ for HNO_3 + soot[18] and $\gamma = 0.064$ for NO_2 + soot[16] were measured. This large deviation may be explained considering the different experimental methods studying amorphous carbon on one hand and GfG soot or diesel soot aerosol on the other hand. For the Knudsen cell method, typically the geometrical surface is used for the calculation of the reactive uptake coefficients. In our experiments the absorbance was approximately linearly dependent on the soot mass, i.e., sample thickness and was independent of the NO_2 concentration (Figure 5), which means that the entire internal surface is available for reaction and not only the geometrical area of the soot spot which is virtually the same for all samples, independent of the soot mass. In a typical Knudsen cell setup the geometrical surface area of soot samples was in the order of 14.9 cm^2 and 6.2 cm^2 for a 1−2 mm layer.[18] This corresponds to a surface area of 10−20 cm^2g^{-1} (at density = 0.5 g/cm^3), which is several orders of magnitude below the BET surface area (460 m^2g^{-1}, manufacturer data). We do not want to conclude that the BET surface should be used in the evaluation of Knudsen cell experiments; however, trapping of gas-phase molecules in the pores and cavities should not be neglected. Therefore, the geometrical surface area will always be a lower limit and the resulting γ values will represent an upper limit.

Conclusions

We show here, that soot samples of different origin have significantly different FTIR spectra: the content of surface OH/C≡C−H/C═O/C−O groups depends strongly on the soot type and sampling conditions. Formation of surface reaction products in the heterogeneous reactions of soot with NO_2 and HNO_3 was observed by FTIR spectroscopy, and reaction rates were determined. We find that the reactivity of soot obtained from a spark discharge generator is nearly 1 order of magnitude larger than that of soot obtained from diesel engine exhaust.

Our experiments show that the kinetics of the NO_2 or HNO_3 reactions with soot can be best fitted by two parallel processes. The reaction order has been determined over a concentration range of $[NO_2] = 1.6 \times 10^{12}$ to 2.4×10^{14} molecule cm^{-3} and $[HNO_3] = 5.4 \times 10^{12}$ to 2.2×10^{14} molecule cm^{-3}. For the NO_2 + soot reaction, we determine values of the reaction order of the slow and of the fast process to be $n_r \approx 0.3$ (± 0.3) and $n_{ini} \approx 0.1$ (± 0.3), respectively. The reaction order of the HNO_3 + soot reaction is $n \pm 0.5$ (± 0.6) for the fast and the slow process. Therefore, the calculated surface reaction probabilities depend on the reactant concentration and should be used only for appropriate conditions. The values decrease with increasing $[NO_2]$ in the range of $\gamma \approx 2 \times 10^{-3}$ to 2×10^{-6} for the fast, and $\gamma \approx 6 \times 10^{-6}$ to 2×10^{-8} for the slow process. Similarly, increasing $[HNO_3]$ gives decreasing surface reaction probabilities in the range of $\gamma \approx 8 \times 10^{-4}$ to 5×10^{-6} for the fast, and $\gamma \approx 2 \times 10^{-6}$ to 1×10^{-7} for the slow process. The surface reaction probabilities can be different to reactive uptake coefficients, if reactions of gas-phase species occur that do not modify the surface. In all experiments we observe surface saturation. Therefore, in atmospheric modeling the aerosol soot surface needs to be treated as a reactant, which is consumed during reaction. This conclusion is true until no significant regenerating of active surface sites, e.g. by reaction with water or other species, has been discovered and if ambient soot aerosol reacts in a manner similar to GfG soot or diesel soot. The effect of water on HONO formation has been documented;[12,15] however, the reaction mechanism is still under discussion because the surface catalyzed heterogeneous reaction $2NO_2 + H_2O \rightarrow HNO_3 + HONO$ was ruled out.[12]

In a recent study, on flame deposited hydrocarbon soot, Longfellow et al.[15] did not observe aging of the soot at experimental time scales in the order of 10 min and NO_2 concentrations of $(0.2-2) \times 10^{12}$ molecule cm^{-3}. Therefore, a catalytic role of active soot sites was suggested for the formation of HONO from the reaction of NO_2 with water. A typical reaction probability of $\gamma \approx 1 \times 10^{-4}$ was found and about 20% of the NO_2 taken up was converted to gas-phase HONO. Longfellow et al.[15] concluded that this reaction could at least partially account for the high HONO levels observed in urban areas.[34] However, these authors also observed a decrease of HONO production with exposure time. This was interpreted as possible evidence for the reaction $NO_2 + H_2O \rightarrow HONO + OH$, in which HONO desorbs and OH deactivates the soot. Scaled with the much longer reaction times and somewhat higher NO_2 concentration used in our experiments, the deactivation described by Longfellow et al.[15] is in the same order of magnitude as the surface saturation observed in this study.

Ammann et al. (1998)[12] have argued that photolysis of HONO formed by reaction of NO_2 with soot particles may be an important source of OH radicals in the atmosphere. Our data and the work of Kamm et al. (1997)[29] and of Kleffmann et al. (1999)[14] show that with the exception of a short initial phase, the interaction of NO_2 with soot is very slow. The observed uptake kinetics are too low to have a significant impact on atmospheric NO_2 or HNO_3 concentrations.[3,35] At long reaction times we observed surface saturation and determine the maximum number of active sites $N_{max} = 2.2 \times 10^{14}$ molecule cm^{-2}. Within the time scale of their experiment Ammann et al. (1998)[12] measured the formation of [HONO] $= 3 \times 10^{14}$ molecule cm^{-2} of spark generator soot. This is reasonably consistent with our upper limit for the possible HONO production of 2.2×10^{14} molecule cm^{-2}, assuming that every reactive surface site has been converted to a HONO molecule. In typical urban air with a soot surface/volume ratio of 3×10^{-5} cm^{-1}, this would give [HONO] $= 9 \times 10^9$ molecule cm^{-3} (0.3 ppbv).[12] Without significant surface reactivation, HONO formation on soot cannot explain the occurrence of up to 14 ppbv of HONO observed during the night time in urban areas.[34]

The coverage of the soot surface with nitrogen containing functional groups may change the physical properties of soot such as light absorption and scattering properties as well as its hygroscopicity. A soot particle aged by exposure to NO_2 or HNO_3 may become a cloud condensation nucleus at lower supersaturations of water vapor as compared to the more hydrophobic, freshly emitted particle. A similar behavior has been observed for soot particles that have been digested in aqueous acids,[9] or particles aged by ozone.[8] Consequently, aged particles may agglomerate faster and may be washed out easier from the atmosphere, thus have a shorter atmospheric lifetime.

Acknowledgment. This work was partially supported by BMBF grant 07AF210A. We also thank Dr. Tim J. Wallington and the two anonymous reviewers for review of the manuscript and very useful comments.

References and Notes

(1) Lary, D. J.; Lee, A. M.; Toumi, R.; Newchurch, M. J.; Pirre, M.; Renard, J. B. *J. Geophys. Res.* **1997**, *102*, 3671.
(2) Hauglustaine, D. A.; Ridley, D. A.; Solomon, S.; Hess, P. G.; Madronich, S. *Geophys. Res. Lett*. **1996**, *23*, 2609.
(3) Aumont, B.; Madronich, S.; Ammann, M.; Kalberer, M.; Baltensperger, U.; Hauglustaine, D.; Brocheton, F. *J. Geophys. Res*. **1999**, *104*, 1729.
(4) Akhter, M. S.; Chughtai, A. R.; Smith, D. M. *Appl. Spectrosc*. **1985**, *39*, 154.
(5) Sergides, C. A.; Jassim, J. A.; Chughtai, A. R.; Smith *Appl. Spectrosc*. **1987**, *41*, 482.
(6) Kerminen, V.−M.; Mäkelä, T. E.; Ojanen, C. H.; Hillamo, R. E.; Vilhunen, J. K.; Rantanen, L.; Havers, N.; von Bohlen, A.; Klockow, D. *Environ. Sci. Technol*. **1997**, *31*, 1883.
(7) Burtscher, H.; Künzel, S.; Hüglin, C. *J. Aerosol Sci*. **1998**, *29*, 389.
(8) Kotzick, R.; Niessner, R. *J. Aerosol Sci.* **1997**, *28*, S165.
(9) Lammel, G.; Novakov, T. *Atmos. Environ.* **1995**, *29*, 813.
(10) Liousse, C.; Penner, J. E.; Chuang, C.; Walton, J. J.; Eddleman, H.; Cachier, H. *J. Geophys. Res*. **1996**, *101*, 19411.
(11) De Santis, F.; Allegrini, I. *Atmos. Environ*. **1992**, *26*, 3061.
(12) Ammann, M.; Kalberer, M.; Jost, D. T.; Tobler, L.; Rössler, E.; Piguet, D.; Gäggeler, H. W.; Baltensperger, U. *Nature* **1998**, *395*, 157.
(13) Gerecke, A.; Thielmann, A.; Gutzwiller, L.; Rossi, M. *J. Geophys. Res. Lett*. **1998**, *25*, 2453.
(14) Kleffmann, J.; Becker, K. H.; Wiesen, P. *Proceedings of the EUROTRAC Symposium '98*; Borrell, P. M., Borrell, P., Eds.; WITpress: Southampton, 1999; 1, 656.
(15) Longfellow, C. A.; Ravishankara, A. R.; Hanson, D. R. *J. Geophys. Res*. **1999**, *104*, 13833.
(16) Tabor, K.; Gutzwiller, L.; Rossi, M. J. *J. Phys. Chem.* **1994**, *98*, 6172.
(17) Kalberer, M.; Tabor, K.; Ammann, M.; Parrat, Y.; Weingartner, E.; Piguet, D.; Rössler, E.; Jost, D. T.; Türler, A.; Gäggeler, H. W.; Baltensperger, U. *J. Phys. Chem*. **1996**, *100*, 15487.
(18) Rogaski, C. A.; Golden, D. M.; Williams, L. R. *Geophys. Res. Lett.* **1997**, *24*, 381.
(19) Chughtai, A. R.; Gordon, S. A.; Smith, D. M. *Carbon* **1994**, *32*, 405.
(20) Smith, D. M.; Chughtai, A. R. *Colloids Surf., A* **1995**, *105*, 47.
(21) Choi, W.; Leu, M. T. *J. Phys. Chem*. **1998**, *102*, 7618.
(22) Smith, D. M.; Welch, W. F.; Graham, S. M.; Chughtai, A. R.; Wicke, B. G.; Grady, K. A. *Appl. Spectrosc*. **1988**, *42*, 674.
(23) Wicke, B. G.; Grady, K. A. *Combust. Flame* **1987**, *69*, 185.
(24) Kamm, S.; Möhler, O.; Naumann, K.−H.; Saathoff, H.; Schurath, U. *Atmos. Environ.* **1999**, *33*, 4651.
(25) DeMore, W. B.; Sander, S. P.; Golden, D. M.; Hampson, R. F.; Kurylo, M. J.; Howard, C. J.; Ravishankara, A. R.; Kolb, C. E.; Molina, M. J. *Chemical Kinetics and Photochemical Data for Use in Stratospheric Modeling*; JPL Publication 97-4, Jet Propulsion Laboratory: Pasadena, CA, 1997.
(26) Chughtai, A. R.; Jassim, J. A.; Peterson, J. H.; Stedman, D. H.; Smith, D. M. *Aerosol Sci. Technol*. **1991**, *15*, 112.
(27) Smith, D. M.; Akhter, M. S.; Jassim, J. A.; Sergides, C. A.; Welch, W. F.; Chughtai, A. R. *Aerosol Sci. Technol*. **1989**, *10*, 311.
(28) Jassim, J. A.; Lu, H. P.; Chughtai, A. R.; Smith, D. M *Appl. Spectrosc.* **1986**, *40*, 113.
(29) Kamm, S.; Möhler, O.; Naumann, K. H.; Saathoff, H.; Schurath, U. *PSI Proceedings* **1997**, *97−02*, 29.
(30) Lide, D. R. *CRC Handbook of Chemistry and Physics*, 78th ed.; CRC Press: Boca Raton, New York, 1997−1998.
(31) Vogt, R.; Elliot, C.; Allen, J. M.; Hemminger, J. C.; Finlayson−Pitts, B. J. *Atmos. Environ*. **1996**, *30*, 1729.
(32) Rothenberg, S. J.; Kittelson, D. B.; Cheng, Y. S.; McCellan, R. O. *Aerosol Sci. Technol*. **1985**, *4*, 383.
(33) Kirchner, U., Börensen, C.; Scheer, V.; Vogt, *R. Proceedings of the EUROTRAC Symposium '98*; Borrell, P. M., Borrell, P., Eds.; WITpress: Southampton, 1999; 1, 666.
(34) Febo, A.; Perrino, C.; Allegrini, I. *Atmos. Environ*. **1996**, *30*, 3599.
(35) Chatfield, R. B. *Geophys. Res. Lett.* **1994**, *21*, 2705.